Journal of Molecular Liquids 307 (2020) 112960

Contents lists available at ScienceDirect

Journal of Molecular Liquids

journal homepage: www.elsevier.com/locate/molliq

Thermal and spectroscopic investigations on three phosphonium based ionic liquids for industrial and biological applications

K.K. Thasneema [a], Mohamed Shahin Thayyil [a,*], Tancia Rosalin [b], K.K. Elyas [b], T. Dipin [c], Pramod K. Sahu [d], N.S. Krishna Kumar [e], V.C. Saheer [f,1], Mouslim Messali [g], Taibi Ben Hadda [h,2]

[a] Department of Physics, University of Calicut, Kerala, India
[b] Department of Biotechnology, University of Calicut, Kerala, India
[c] Department of Chemistry, University of Calicut, Kerala, India
[d] School of Study in Chemistry, Jiwaji University, Madhya Pradesh, India
[e] Department of Pharmaceutics, University of Minnesota, USA
[f] Department of Chemistry, IIT Madras, Tamilnadu, India
[g] Department of Chemistry, Faculty of Science, Taibah University, Saudi Arabia
[h] Faculty of Sciences, University Mohammed Premier, Oujda 60000, Morocco

ARTICLE INFO

Article history:
Received 9 July 2019
Received in revised form 18 February 2020
Accepted 20 March 2020
Available online 22 March 2020

Keywords:
Ionic liquids
Broadband dielectric spectroscopy
Thermal analysis
Anti-bacterial activity
Anti-cancer activity

ABSTRACT

We report a comprehensive result of investigations on three phosphonium based room temperature ionic liquids (ILs) of same cation, trihexyltetradecylphosphonium ($[PC_6C_6C_6C_{14}]$), with different anions *viz.* chloride $[-Cl]^-$ $[Cl]^-$, dicyanamide $[-N(CN)_2]^-$ and bis(trifluoromethylsulfonyl) imide $[-NTf_2]^-$ for catching the effect of size, symmetry, dipole moment, as well as electro-negativity of anions on glassy dynamics and charge transport of the formed ILs. The effort was made for tuning the property for getting superior conductivity, improved thermal stability, better electrode-electrolyte interaction to enable it for diverse biological and technological applications. The ILs were characterized with differential scanning calorimetry (DSC), thermogravimetry (TGA), broadband dielectric spectroscopy (BDS) along with other routine measurements like FT-IR, FT-Raman spectroscopies and computational investigations with density functional theory (DFT). The applications were evaluated by means of electrochemical and biological activities. From DSC and TGA measurements, the samples showed good thermal stability up to 573 K to project them as excellent electrolyte and better heat transfer fluid for high temperature needs in various technological fronts. Dielectric response revealed that the conductivity relaxation manifested above glass transition temperature (Tg) to be well represented by Dyre's random barrier model and it followed a Vogel–Fulcher–Tamman (VFT) behaviour against temperature. The sub-Tg relaxation reflected a Cole-Cole response with an Arrhenius T-dependence. The dielectric data revealed a slight correlation with Tg while anticorrelates with the fragility and low temperature activation energy (E_β). The DFT calculations gave the structure and other parameters in good agreement with the experimental data. The three ILs fulfilled most of the requirements needed for pharmaceuticals on evaluating pharmacokinetics, bioavailability and toxicity *via in silico* analysis. On exploring the preliminary biological studies, these ILs showed very good anti-bacterial, anti-oxidant and good anti-cancer activities highlighting their relevance and significance for pharmaceutical applications.
© 2020 Elsevier B.V. All rights reserved.

1. Introduction

Ionic liquids (ILs) are molten salts composed of a cation (aromatic or occasionally non-aromatic) and an anion of organic or inorganic in origin [1]. ILs received a wider acceptance and popularity in fundamental research as well as in industrial fronts owing to their novel properties like high thermal and chemical stability, low volatility, lack of inflammability as well as improved solubility vis-à-vis to many organic compounds [1–4]. Room temperature ionic liquids (RTILs) whose melting temperature is below room temperature were emerged as greener alternatives to many of the traditional volatile organic solvents with innumerable potentials and capabilities for diverse technological interests *viz.* synthetic reactions, separations and extractions, electrochemical, nanotechnological, biotechnological, and engineering processes [1–4]. Depending on the cation segment the ILs are named and categorized as ammonium, imidazolium, phosphonium, pyridinium, pyrazolium, pyrrolidinium, cholinium, sulfonium, picolinium, piperidinium,

* Corresponding author.
E-mail address: shahin@uoc.ac.in (M.S. Thayyil).
[1] Department of Chemistry, Krishna Menon Memorial Government Women's College Kannur,Kerala, India - 670004.
[2] Department of Pharmaceutical Chemistry, Faculty of Pharmacy, Umm Al-Qura University, Makkah Almukkarramah, Saudi Arabia.

https://doi.org/10.1016/j.molliq.2020.112960
0167-7322/© 2020 Elsevier B.V. All rights reserved.

thiazolium, triazolium, guanidinium *etc*. [2,5]. Among these, the first four are the most commonly used ILs. Judicious combinations of appropriate cations and anions by exploring their fascinating chemistry in a way by varying size, symmetry and attached side groups *etc*., a huge database of useful ILs have evolved with diverse dynamical and transport properties for a range of novel applications [6]. In fundamental research, ILs are appealing due to the dual advantage of ionic conductivity and glass forming nature, which opens up an apt avenue to investigate fundamental queries on the dynamics of ionically conducting glass-formers in their supercooled liquid and glassy states [6–11]. The glass transition temperature (Tg) has a direct influence on conductivity of ILs as reflected in its dependence on viscosity, mobility and charge transport. The Tg characterizes the time scale of molecular mobility approximately equals to 100 s or the viscosity reaches to about 10^{12} Pa.s [6–11].

Midst the popularly used ILs, phosphonium based ILs are more innovative for reactions carried out above 100 °C owing to their higher thermal stability, apt catalytic and solvent activity [2,12]. They can be used as powerful phase-transfer catalysts for many reactions *viz*. Halex, Heck and Suzuki reaction *etc*. [13]. Wide electrochemical window seen in phosphonium based ILs opens a favourable opportunity to develop efficient supercapacitors for energy storage applications which can cater domestic as well as industrial demands [12]. In biological arena, ILs show anti-bacterial, anti-oxidant and anti-cancer activities resulting from their high ionic nature, tunability in their structure and other novel attributes which were demonstrated by *in vitro* studies in human cell lines [14–20]. Further, ILs can also be used for a variety of bio-applications like biosensors, protein stabilization and bio-preservation *etc*. [4]. In addition to the above, phosphonium based ILs are more effective with less cytotoxicity compared to other common ILs [21,22].

In this piece of work, we demonstrate *via* experimental investigations on three phosphonium based ILs having a common cation $[PC_6C_6C_6C_{14}]$ with different anions *viz*. $[\text{-Cl}]^-$, $[\text{-N(CN)}_2]^-$,and $[\text{-NTf}_2]^-$ to get a comprehensive picture on how the dynamics is varied with the increase of molecular mass, ionic conductivity, and electronegativity. Molecular dynamics on changing the temperature was thoroughly investigated by broadband dielectric spectroscopy and thermal response was done by DSC and TGA. The biological activity was evaluated with respect to anti-bacterial, anti-oxidant and anti-cancer properties. To verify the drug likeness of the ILs, *in silico* analysis, along with toxicity risk and pharmacokinetic investigations were also performed.

2. Experimental section

2.1. Materials and methods

The phosphonium based ionic liquids $[PC_6C_6C_6C_{14}][Cl]$ MW = 519.31 g mol^{-1}, $[PC_6C_6C_6C_{14}]$ $[N(CN)_2]$, MW = 549.90 g mol^{-1} and $[PC_6C_6C_6C_{14}][NTf_2]$ MW = 764 g mol^{-1} were purchased from M/s. Sigma Aldrich, USA with specific purity >98%. All ILs were used as received without further purification. The chemical structures were shown in Fig. 1.

2.2. Thermal and vibrational analysis

To get an initial overview about the thermal responses of the ILs, thermogravimetry analysis (TGA) and differential scanning calorimetry (DSC) were performed. TGA measurement to ascertain thermal stability and degradation of IL was carried out using Perkin Elmer TGA Q50 instrument. DSC measurement was done using a Mettler Toledo DSC 822e calorimeter. The instrument was calibrated for temperature and specific heat using indium as standard. The IL was placed inside a sealed aluminum pan and cooled to deep glassy state and measurements were recorded during heating from 123 K to room temperature at heating rate of 10 K min^{-1}. Vibrational analysis was done with FT-IR spectrometer (JASCO 4100) using KBr pellets. Raman spectra were recorded with Bruker MultiRAM FT-Raman spectrophotometer. Theoretical calculations corresponding to FT-IR and FT-Raman were evaluated using density functional theory (DFT) with Gaussian 09 package [2]. The calculations were optimized by RB3LYP with LANL2DZ basis set.

2.3. Dielectric measurements

Dielectric measurements at ambient pressure by changing temperatures were carried out using a broadband dielectric spectrometer (Novocontrol Alpha Analyser, Novocontrol technologies, Germany). The samples were kept between two circular stainless steel electrodes of 30 mm effective diameter separated 100 μm apart with two narrow Teflon spacers achieving an empty cell capacitance of appr. 60 pF. The measurements were covered in a frequency range of 10^{-2}–10^{7} Hz and a temperature range from 123 K to 298 K. The temperature was controlled with dry nitrogen purge using a Quatro cryosystem (Novocontrol technologies, Germany) achieving a stability better than 0.1 K. The applied ac electric field is 1 V. The samples were carefully poured in to the dielectric cell, placed in the cryosystem and quenched to 123 K by recording the isochronal data at few frequencies to ascertain the nature of cooling and ensure a smooth transit towards the glassy state and the isothermal dielectric measurements were recorded during heating after stabilizing the sample at the set temperature for about 600 s [2].

2.4. Biological activities

2.4.1. Anti-bacterial activity

The *in vitro* anti-bacterial activity of the ILs were tested against two common bacterial strains *viz*. *E. coli* and *S. aureus* by agar disc diffusion method. The inocula of the selected bacterial species were prepared from fresh overnight broth cultures (Tripton soy broth with 0.6% yeast extract-Torlak, Serbia) which were incubated at 37 °*C* with a constant stirring and used for diffusion studies. The diffusion technique was carried out by pouring agar into Petri dishes to form 4 mm thick layers and adding a dense inocula of the test organisms of two strains in order to obtain a better growth. Petri plates were left for 10 min. in a laminar air flow and discs (6 mm) were prepared from Whatman no. 3 filter paper, immersed into different volumes having 0.0, 2.5, 5.0, 7.5 and 10 (μg mL^{-1}) of the samples, placed at equal distances and then incubated further at 37 °*C* for overnight in a bacteriological incubator. The results were obtained by measuring the width of the zone of inhibition in millimeter around the disc which was produced by the sample against the two bacterial strains [14,16,23].

2.4.2. Anti-oxidant assay

The 1,1-diphenyl-2-picryl hydrazyl (DPPH) radical scavenging activity was carried out as per Brand–Williams et al. protocol with a slight modification. Different concentrations of the samples were prepared in methanol. 0.1 mM methanolic solution of DPPH was added to these samples and absorbance was measured at 517 nm followed by 30 min. incubation in the dark. Ascorbic acid was used as standard. All measures were done in triplicate. The DPPH scavenging activity was calculated as [17–20].

$$\%\text{DPPH scavenging activity} = \frac{\text{A control} - \text{A sample}}{\text{A control}} \times 100$$

Thus, IC_{50} concentration which is required to obtain a 50% anti-oxidant effect was determined.

2.4.3. Anti-cancer activity

2.4.3.1. Cell lines and cell culture. Four cancer cell lines: A549 (Human lung cancer), K562 (chronic myelogenous leukemia), Jurkat E6-1 (leukemic T cell lymphoblast) and HCT 116 (colorectal carcinoma) were obtained from National centre for cell science (NCCS), Pune, India. HCT 116

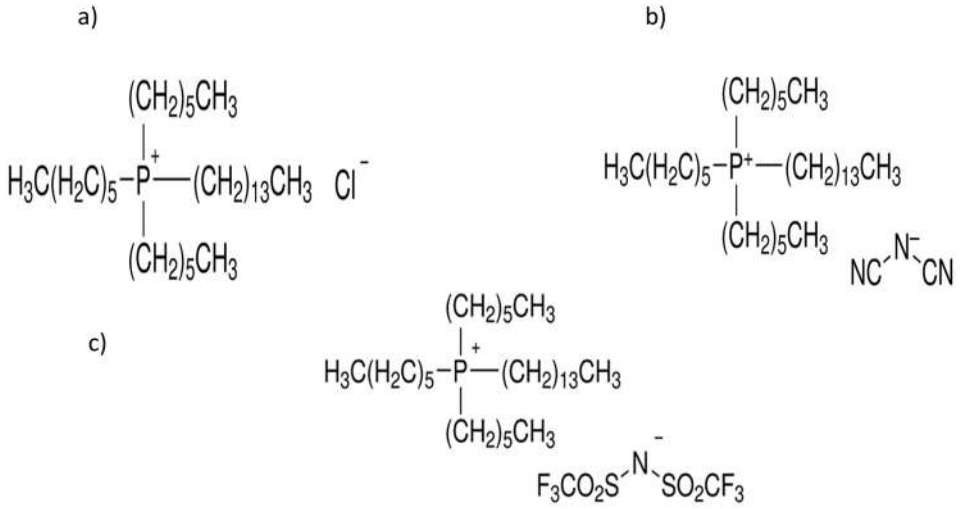

Fig. 1. Chemical structures of (a) $[PC_6C_6C_6C_{14}][Cl]$ (b) $[PC_6C_6C_6C_{14}][N(CN)_2]$ and (c) $[PC_6C_6\ C_6C_{14}][NTf_2]$ ILs.

was cultured in Dulbecco's modified Eagles medium, while K562 and Jurkat E6-1 were maintained in RPMI-1640. Both Dulbecco's modified Eagles medium and RPMI media were supplemented with 10% fetal bovine serum, streptomycin (100 μg mL^{-1}) and penicillin (50 IU/mL). A549 was maintained with 2 mM L-glutamine and Earle's basal salt solution adjusted to contain 1.5 g L^{-1} Na bicarbonate, 0.1 mM non-essential amino acids, and 1.0 mM of Na pyruvate. Cells were cultured in a humidified atmosphere containing 5% CO_2 at 37 °*C* [15,21,22,24].

2.4.3.2. Cell viability assay. The effect of ILs on cell viability was determined using, 3-(4,5-dimethylthiazol-2-yl)-2,5-diphenyltetrazolium bromide (MTT) assay. Briefly, 10,000 cells/well were seeded into a 96 well tissue culture plate and incubated overnight in CO_2 incubator at 37 °*C* in 5% CO_2 atmosphere under humidified condition. Subsequently, a fresh medium containing varying concentrations of the IL was added to each well and incubated for 48 h. After incubation, the media was aspirated and replaced with a fresh medium. MTT (5 mg mL^{-1}) dissolved in phosphate buffered saline (PBS) was added to each well, and the plates were incubated for further 4 h at 37 °*C* in dark. After removing the medium, the formazan crystals formed were dissolved in DMSO and the cell growth condition was reflected by the color intensity of the formazan solution. Absorbance at 570 nm was taken on a 96-well microplate reader (MD VERSA max). The half maximal inhibitory concentration of proliferation (IC_{50}) values for samples on each cancer cell line was calculated as the average of three independent experiments [15,21,22,24]. The optical density (OD) value, i.e., the absorbance at 570 nm wavelength, was used to calculate the percentage of viability using the formula [15,21,22,24].

$$\%\text{of cell viability} = \frac{\text{OD value of experimental sample}}{\text{OD value of experimental control}} \times 100$$

2.5. In silico analysis

The pharmacokinetic profile (i.e.: absorption, distribution, metabolism, excretion and toxicity (ADMET)), topological polar surface area (TPSA), clogP, fragment-based drug likeness and drug score values of the three ILs were predicted using *in silico* economic and efficient bioinformatics tools *viz*. admetSAR and ADME [25,26].

3. Results and discussions

3.1. Computational studies

DFT calculations using Gaussian 09 package on all the explored anions were carried out at RB3LYP level of theory with LANL2DZ basis set to ascertain the structural and 3D details (bond lengths & bond angles) and their possible interactions. The results were shown in Fig. 2 (a & b) and in Table I. From Table I, it is inferred that for the smaller anion, $[PC_6C_6C_6C_{14}][Cl]$ has the highest dipole moment and was reflected in its high melting point among the investigated ILs.

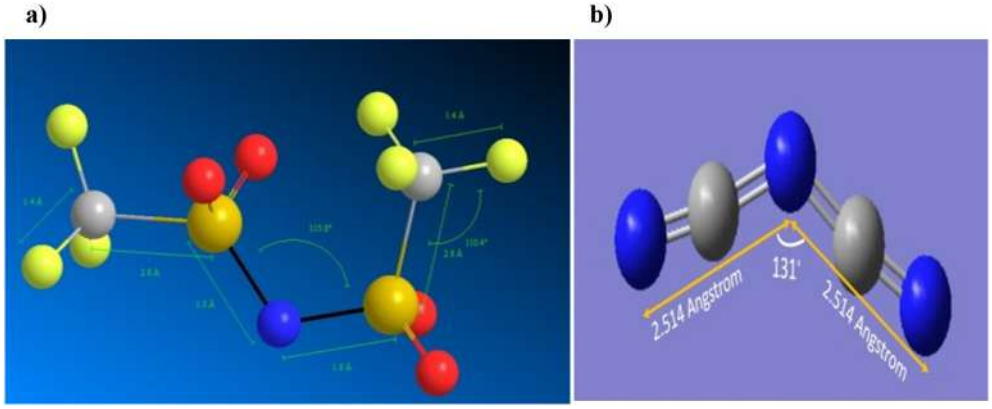

Fig. 2. Bond lengths and bond angles of (a) $[-NTf_2]^-$ and (b) $[-N(CN)_2]^-$ anions using DFT calculation at RB3LYP method using Gaussian 09 package.

Table I
Bond lengths and bond angles of (a) $[-N(CN)_2]^-$ and (b) $[-NTf_2]^-$ anions.

Ionic liquids	Dipole moments (Debye)	Bond lengths (Å)	Bond angles (degree)
$[PC_6C_6C_6C_{14}][Cl]$	15.01		
$[PC_6C_6C_6C_{14}][N(CN)_2]$	11.99	C-N (1.257)	C-N-C(131)
$[PC_6C_6C_6C_{14}][NTf_2]$	13.89	N-S(1.8)	S-N-S(115.0)
		C-S(2.0)	S-C-F(110.4)
		C-F(1.4)	
		S-F(2.0)	

Interestingly, dicyanamide anion $[-N(CN)_2]^-$ possesses a unique structure with two nitrogen atoms symmetrically arranged about the third N atom which effectively reduces the dipolar interaction and has the lowest dipole moment.

3.2. Vibrational analysis

Experimental values of FT-IR spectra and FT-Raman spectra along with the DFT calculations of the three ILs are shown in Figs. 3(a, b & c) and 4(a, b & c) respectively, which delivered a detailed structural information and on the functional groups attached to the ILs. Details about different peaks were given in the supplementary data for further reference. Theoretical calculations of FT-IR and FT-Raman frequencies showed the actual trend in experimental observation with most of the stretching frequencies appeared in the theoretical calculations. The comparison of theoretical and experimental IR frequencies shown in the supplementary data also confirm this observation even though there is a little shift in frequencies of computed data. Comparison is more appealing for FT-Raman spectra than FT-IR.

3.3. Thermal analysis

Thermal properties of the ILs were investigated by TGA followed by DSC. TGA measures the changes in weight of a sample in a controlled heating program while DSC records the amount of heat energy absorbed/liberated by it. This technique is further used for thermal

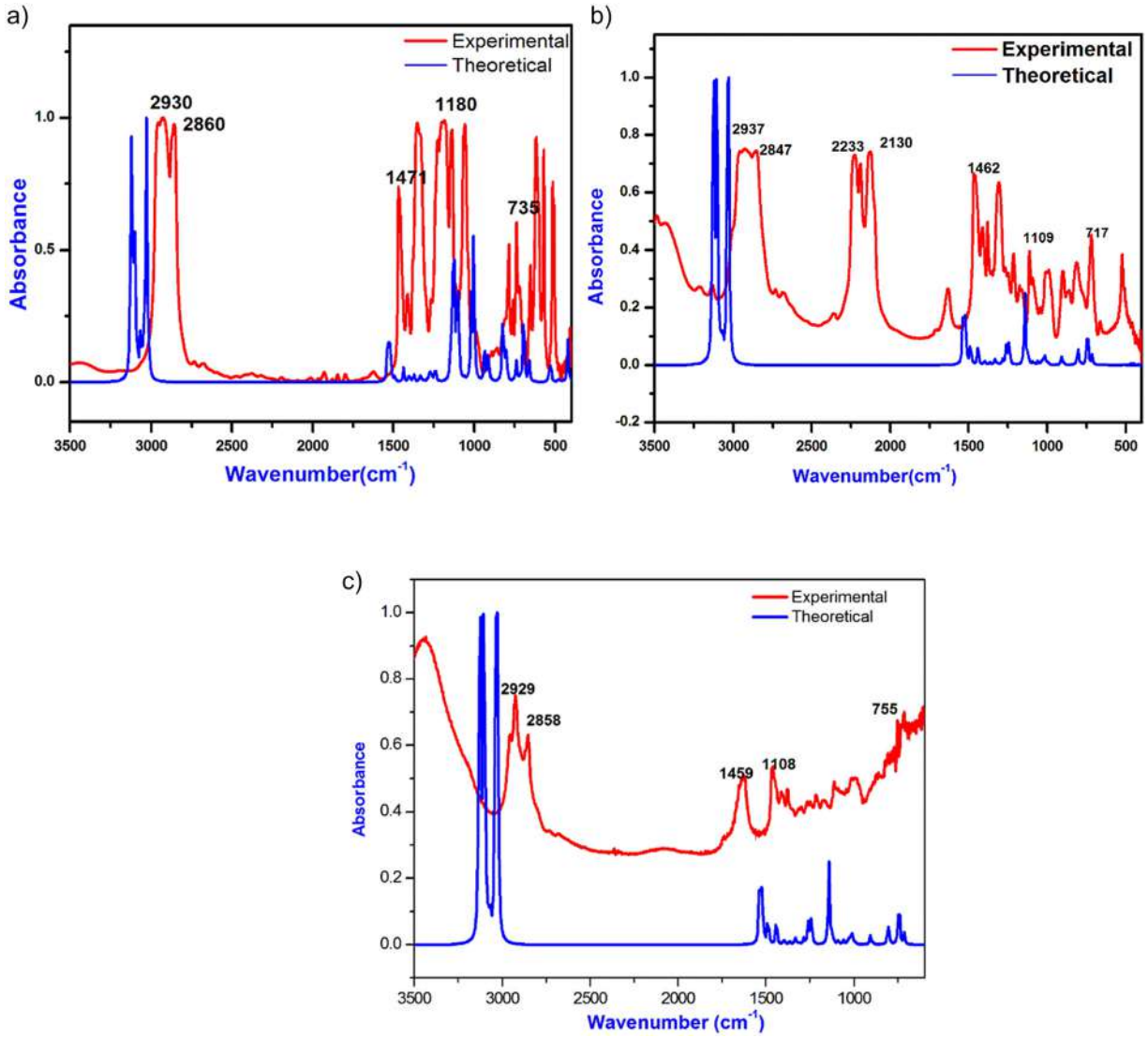

Fig. 3. Experimental and theoretical FT-IR spectra of (a) $[PC_6C_6C_6C_{14}][NTf_2]$ (b) $[PC_6C_6C_6C_{14}][N(CN)_2]$ and (c) $[PC_6C_6C_6C_{14}][Cl]$ ILs.

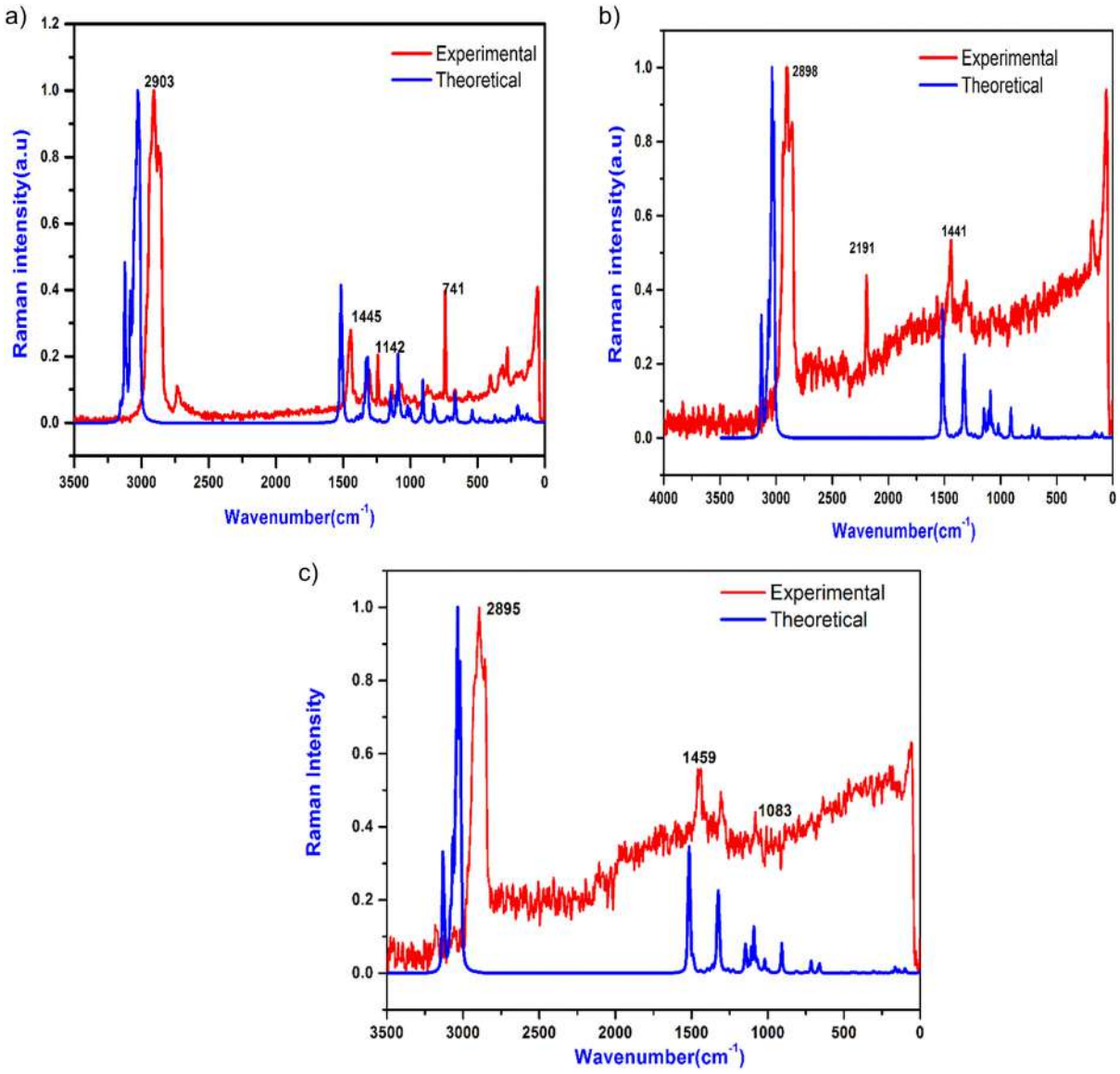

Fig. 4. Experimental and theoretical FT-Raman spectra of (a) $[PC_6C_6C_6C_{14}][NTf_2]$ (b) $[PC_6C_6C_6C_{14}][N(CN)_2]$ and (c) $[PC_6C_6C_6C_{14}][Cl]$ ILs.

decomposition studies and to assess the upper temperature limit of a sample for practical applications. It had already been reported that the experimental conditions such as heating environment, scanning rate and sample mass can considerably affect TGA response and decomposition. TGA plots of the ILs are shown in Fig. 5(a) and the details are given in Table II. From the figure and the table, it is revealed that the cation has a decisive role indicating the interaction, which resulted in obtaining an enhanced thermal stability for the three ILs up to about 573 K ($Td_{1\%}$). For getting an idea on the rate of decomposition, we have figured out the percentage decomposition at three values (5%, 10% and 20%) against the temperature of the three ILs in Table II along with other ILs already reported by others [27–29]. It is worth to note that the stability of IL against thermal degradation may be attributed to the strength of chemical interaction between the ions evolved from the structure of IL and hence differs with different anion–cation combinations.

DSC curves at a heating rate of 10 K $min.^{-1}$ from 123 K to room temperature (heating cycle) were shown in Fig. 5(b) & (c). The slight deviation in the DSC plots is due to the base line mismatch and does not in any way affect the transition temperatures. All the three samples could be supercooled at a normal cooling rate of 10 K $min.^{-1}$ without any indication of crystallization. The heating curve showed a step-like change indicating the glass transition. As shown in Table II, an anti-correlation between the IL size and Tg were noted in the phosphonium based ILs and same trend in the results were also seen in imidazolium cation based ILs reported by others [27–29]. DSC plots did not show any indications of cold crystallization during the subsequent heating from the glassy state, and hence obviously no melting peak could be seen at the melting region.

3.4. Dielectric measurements

Broadband dielectric spectroscopy (BDS) is a powerful experimental tool to study the molecular dynamics for investigating charge transport and the rotational fluctuations of molecular dipoles. Response of dipoles at different length scales to the applied electric field provides a link between the molecular motions and the dielectric function. By extracting complex impedance ($Z^*(\omega) = Z'(\omega) - iZ''(\omega)$) and transforming to appropriate representations *viz*. permittivity ($\varepsilon^*(\omega) = \varepsilon'(\omega) - i\varepsilon''(\omega)$), conductivity ($\sigma^*(\omega) = \sigma'(\omega) + i\sigma''(\omega)$) and electric modulus ($M^*(\omega) = M'(\omega) + iM''(\omega)$) and the dynamics can be inferred [30–34]. This technique can be used to explore different phases like solids, liquids, gases as well as their chemical constituents such as monomer, polymer, ionic systems *etc*. The developments in instrumentation during the last three decades enabled the scientific community to explore dielectric

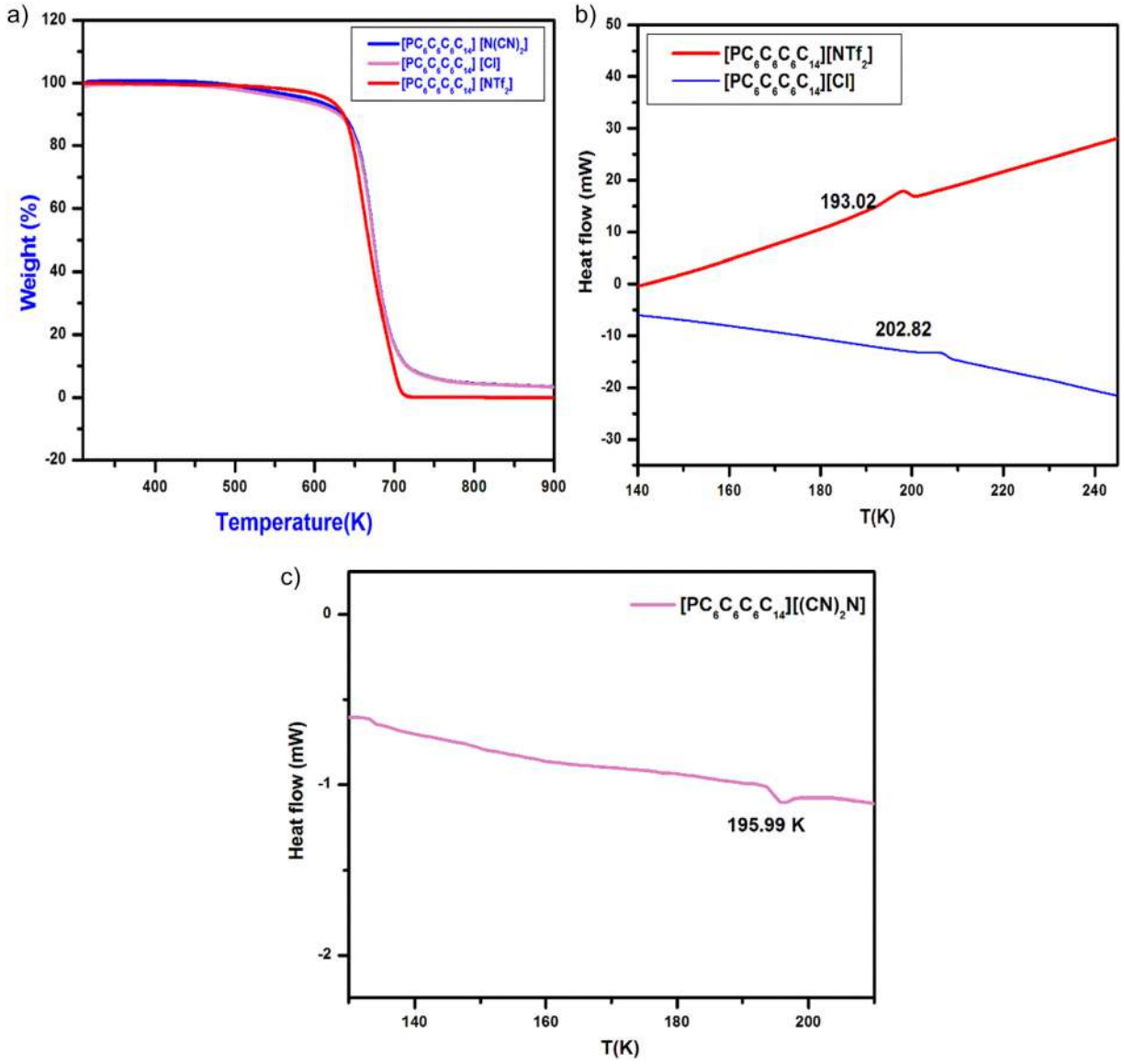

Fig. 5. TGA and DSC response of the three ILs: (a) TGA (b) & (c) DSC.

response in an immense wide frequency and by varying temperature/pressure, and a rich data on various dynamic processes and their inter-relationship could be elucidated. Here, we have explored the charge transport and conductivity relaxation in a frequency window from 10^{-2} to 10^{7} Hz covering deep glassy state to their respective melting temperatures and the results were given in Fig. 6 [2,30–34]. The relation connecting the different representations is: $\sigma^*(\omega) = i\omega\varepsilon_0\varepsilon^*(\omega)$ and $M^*\omega = \frac{1}{\varepsilon^*\omega} = \frac{i\omega\varepsilon_0}{\sigma^*\omega}$, where ε_0 is the dielectric permittivity of free space [30–34]. The three formalisms highlight different aspects of the same underlying mechanism and preference to a representation is given when details are readily obvious over others. In permittivity representation, the real part corresponds to the energy stored in the system, while the imaginary part relates to the energy dissipated by the system. The conductivity quantifies the microscopic movement of ions in macroscopic terms. The modulus has the benefit of blocking the contributions of charge carriers and is mathematically represented as [30–34],

$$M'(\omega) = \frac{\varepsilon'(\omega)}{(\varepsilon'(\omega))^2 + (\varepsilon''(\omega))^2} = \frac{\varepsilon_0\omega\sigma''(\omega)}{(\sigma'(\omega))^2 + (\sigma''(\omega))^2}$$

$$M''\omega = \frac{\varepsilon''(\omega)}{(\varepsilon'(\omega))^2 + (\varepsilon''(\omega))^2} = \frac{\varepsilon_0\omega\sigma'(\omega)}{(\sigma'(\omega))^2 + (\sigma''(\omega))^2}$$

The impedance response of the three ILs at a representative temperature $T = 225$ K above their respective Tgs were shown in Fig. 6. From the figure, the top panels correspond to the real and imaginary parts of the permittivity (ε' and ε''). The real part, ε' shows up at lower frequencies due to the blocking of charges resulting from the electrode polarization and this should not be interpreted as the energy stored in the

Table II
Thermal properties of the ILs with their glass transition temperatures (Tg) and decomposition temperatures (Td) [27–29].

Ionic liquids	T_g (K)	$T_{d\ (onset)}$ (K)	$T_{d\ (5\%)}$ (K)	$T_{d\ (10\%)}$ (K)	$T_{d\ (20\%)}$ (K)
$[PC_6C_6C_6C_{14}]$ [NTf2]	193.02	685.5	616.1	636.1	648.2
$[PC_6C_6C_6C_{14}]$ $[N(CN)_2]$	195.99	679.1	592.0	635.1	654.7
$PC_6C_6C_6C_{14}]$ [Cl]	202.82	666.3	570.5	630.4	653.7
$[C_2MIM]$[NTf2]	181	723	686	705	718
$[C_4MIM]$[NTf2]	187	695	698	702	709
$[C_4MIM]$ $[N(CN)_2]$	183	573	381	453	470
$[C_4MIM]$[Cl]	204	537	302	458	491

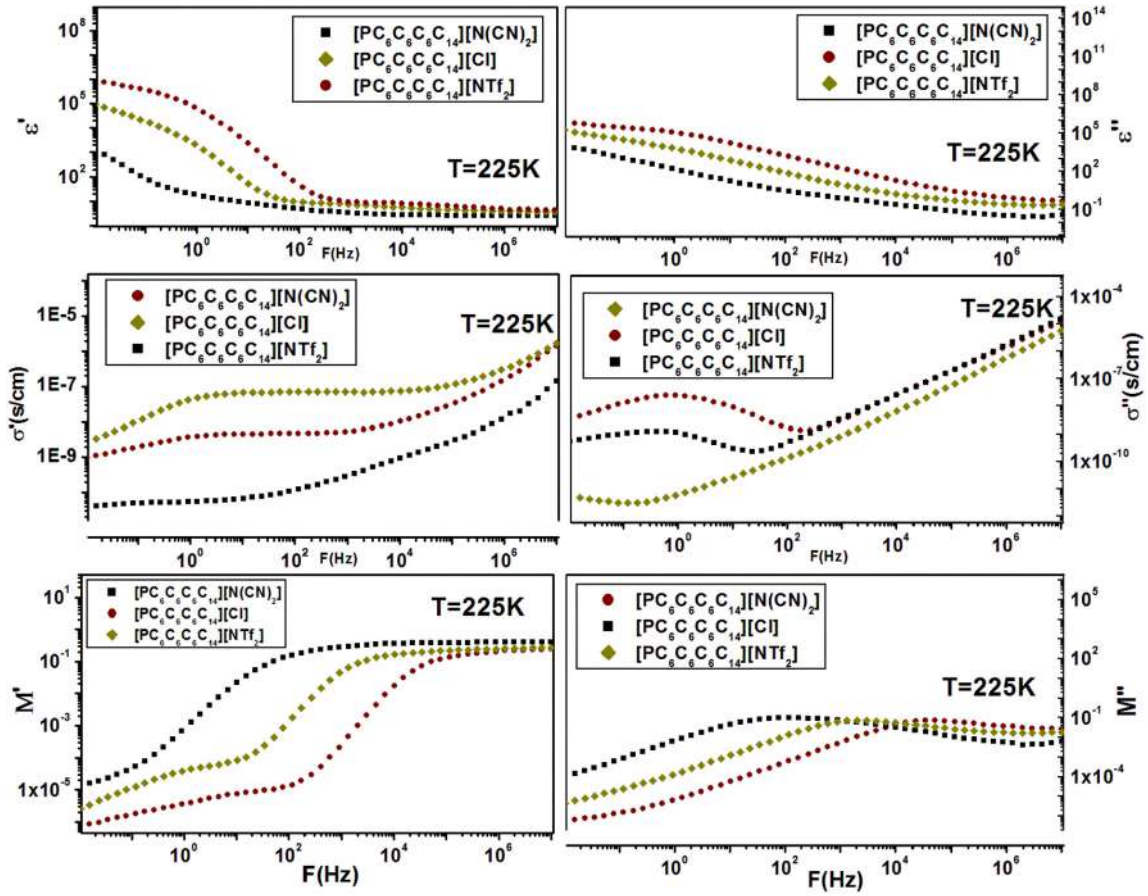

Fig. 6. Plots of ε', ε'', σ', σ'', M′ and M′′*vs* frequency of $[PC_6C_6C_6C_{14}][NTf_2]$, $[PC_6C_6C_6C_{14}]$ $[N(CN)_2]$ and $[PC_6C_6C_6C_{14}][Cl]$ at a test temperature, $T = 225$ K.

system. From the imaginary part ε'', we are unable to resolve the loss peak due to masking of dc conductivity originating from translational movement of ions. The peaks of ε'' and M'' shift to higher frequencies with temperature, but the value of frequency indicate higher in permittivity representation as compared to the modulus representation [30–35].

From the conductivity plots, it is evident that the ac conductivity plateau corresponds to the long-range dc conductivity σ_0 arising from the random diffusion of ionic charge carriers *via* activated hopping. The conductivity drop observed in the lower frequency side of the plateau is due to the blocking of ionic carriers at the electrodes. This phenomenon is characteristic of ionic charge transport and would be absent in electronically conducting solids [30–35]. On moving towards higher frequencies, the conductivity becomes frequency dependent showing a positive slope (power-law) and the plateau crosses over to a dispersive regime from correlated forward–backward motion of ions. The frequency dependence of the conductivity can be explained by Jonscher's universal power law($\sigma_{ac} = \sigma_0 + A\omega^s$) [35], where, A is a temperature dependent parameter and s is the frequency exponent having its value between $0 < s \leq 1$ for ion conducting materials [35]. For further details, readers can refer to our previous publication [2]. As one can see, in Fig. 6 when the temperature increases, σ_0 also increases and the power law region moves out of the experimental window. On comparing the data σ' of the ILs, the conductivity is more for $[\text{-N(CN)}_2]^-$ followed by $[\text{-NTf}_2]^-$ and the least is for $[\text{-Cl}]^-$. The data show that the conductivity is more dependent upon the dipole moment of the ionic liquid rather than the size of the anion.

The real and imaginary parts of electric modulus were also shown in the above figure (lower panel). The characteristic relaxation time of conductivity process can be extracted from the imaginary part M′′ by taking the inverse of the crossover frequency [30–35], which is nothing but the maxima of the modulus loss peak. Here, the crossover manifests as a relaxation in the imaginary part and a step in the real part [30–35]. The dielectric response of all the three ILs in the charge transport regime is well described by the random barrier model of J. C. Dyre, where the charge transport is explained due to hopping of charge carriers in a random spatially varying potential landscape [30–35]. According to this model, the dielectric permittivity is written as [30–35]

$$\varepsilon^*\omega = \varepsilon_\infty + \left(\frac{\sigma_0\tau_e}{\varepsilon_0(\ \ln(1+i\omega\tau_e))}\right)$$

where ε_∞ is the high frequency relaxed value of ε'. Here, the dc conductivity (σ_0) is the highest energy barrier that must be overcome to attain an infinite collection of hopping sites and τ_e the corresponding time [30–35]. On further resolving into real and imaginary parts, we get

$$\varepsilon'\omega = \varepsilon_\infty + \left(\frac{\sigma_0\tau_e \ln(1+\omega^2{\tau_e}^2)}{\frac{1}{2}\varepsilon_0\left(\ln(1+\omega^2{\tau_e}^2)\right)^2 + 2\varepsilon_0(\arctan\ (\omega\tau_e))^2}\right)$$

$$\varepsilon''\omega = \left(\frac{\sigma_0\tau_e \arctan(\omega\tau_e)}{\frac{1}{4}\varepsilon_0\left(\ln(1+\omega^2{\tau_e}^2)\right)^2 + \varepsilon_0(\arctan(\omega\tau_e))^2}\right)$$

Subsequently, the conductivity is obtained as [30–35]

$$\sigma^*\omega = \sigma_0\left(\frac{i\omega\tau_e}{\ln(1+i\omega\tau_e)}\right)$$

On resolving the real and imaginary parts [35],

$$\sigma'\omega = \left(\frac{\sigma_0\omega\tau_e \arctan(\omega\tau_e)}{\frac{1}{4}(\ln(1+\omega^2{\tau_e}^2))^2 + (\arctan(\omega\tau_e))^2}\right)$$

$$\sigma''\omega = \left(\frac{\sigma_0\omega\tau_e \ln(1+\omega^2{\tau_e}^2)}{\frac{1}{2}(\ln(1+\omega^2{\tau_e}^2))^2 + 2(\arctan(\omega\tau_e))^2}\right)$$

To explore the temperature dependence of charge transport quantities σ_0 and the conductivity relaxation time τ_e, we have plotted them in Fig. 7. At temperatures above Tg, both the quantities follow the time honoured Vogel—Fulcher–Tammann (VFT) equation given by [30–35]

$$\tau(T) = \tau_\infty \exp\left(\frac{B}{T-T_0}\right)$$

where τ_∞ is the high temperature limit of the conductivity relaxation time. The VFT equation is widely used for fitting the conductivity data to get quantitative information about the glass-forming behaviour of ILs. The glass transition temperature Tg is normally defined as the temperature at which τ_α (T) ≈ 100 s and is usually adjacent to the value determined by calorimetry. B is the fitting parameter controlling the curvature. B = D T_0, where T_0 is the Vogel temperature commonly appears about 50 to 70 K below T_g. The dc conductivity σ_0 also follows the equation [30–35],

$$\sigma(T) = \sigma_\infty \exp\left(-\frac{B}{T-T_0}\right)$$

where σ_∞ is the high temperature limit of the conductivity. Below Tg τ_e and σ_0 exhibit an Arrhenius temperature dependence given by [2,36]

$$\tau_\beta T = \tau_\infty \exp\left(\frac{E_\beta}{RT}\right)$$

here τ_∞ is the pre-exponential factor, E_β is the activation energy and R is the universal gas constant. The fitting parameters of the three samples were given in Table III along with the T_g obtained from the DSC measurements. From Figs. 7 and 8, the conductivity relaxation time τ_e, increases with decrease in temperature, while the dc conductivity σ_0 shows a thermally activated behaviour [2,33–35]. These results matches with the observations reported by Sangoro et al., who studied the charge transport of imidazolium based ILs with [HMIM] (1-hexyl-3-methyl imidazolium) as cation clubbing with different anions *viz*. [-Cl]$^-$, [-Br]$^-$, [-I]$^-$, [-BF_4]$^-$ and [-PF_6]$^-$ showing universal features of charge transport in these ILs [30,33–35,37].

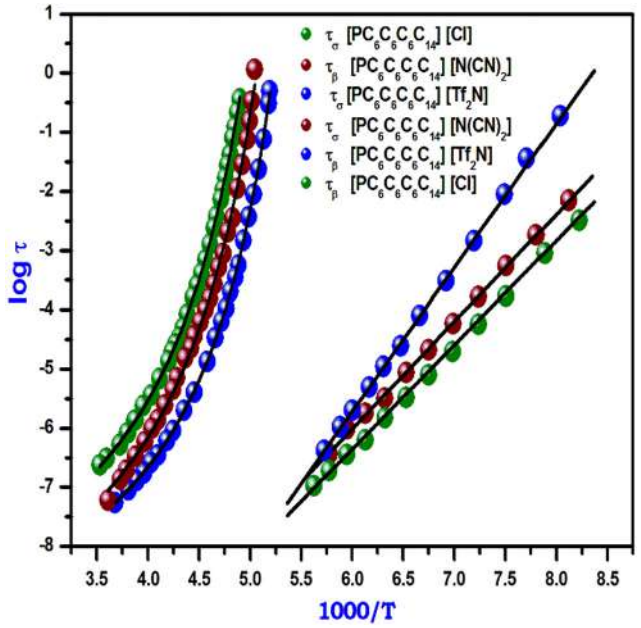

Fig. 7. Plots of 1000/T (K^{-1}) *vs* log τ(s).

Finally, it is intuitive to calculate the fragility or steepness index for getting further insights into various structural features and intermolecular interactions collectively contribute to the overall stability of amorphous phase of the three ILs. The fragility (m) is calculated using the equation proposed by Angell [2,36]

$$\mathrm{m} = \frac{d\log_{10}\tau_\sigma}{d\left(\frac{T_g}{T}\right)}\Big/_{T=Tg}$$

According to Angell's criteria, amorphous systems are classified into strong or fragile based on the systematic deviation from the Arrhenius behaviour [37–39]. A meaningful theoretical framework has been proposed by H. Tanaka in his two order parameter (TOP) model [37–39]. This model proposes that, a competition exists between long-range density ordering leading to crystallization and short-range ordering promoting formation of locally preferred structures not consistent with the crystal geometry [37–39]. When the former dominates, the system eventually favours crystallization. In contrast, if the later effect leads, the system become frustrated and inhibits the crystallization [31,37–39].

Consequently, the fragility may be explained as a measure of degree of frustration and greater the fragility, the system has more tendency for recrystallization as expected [31]. Further, a quantitative deduced parameter ($D = B/T_0$) is evaluated, which expresses the degree of deviation from the Arrhenius nature [36]. Strong systems have a value of D > 25, while fragile ones have value D < 10 [36]. Fragility is also an important parameter useful for predicting the stability of a system against recrystallization during the storage of amorphous materials and glassy pharmaceuticals for packing and preservation, though this property is not much relevant for ILs [31]. The fragility plot of the three ILs is shown in Fig. 9. These ILs show considerable deviation from the Arrhenius behaviour and can be classified as fragile systems [31,36]. Further on comparing the figure and the Table III, it is interesting to note that, fragility increases slightly with the size of the anion, while Tg and T_0 were showed a minor decrease. Remarkably, all parameters show a similar dependency on molecular weight. Thus, it can be concluded that the cation is highly influenced than the anion in these ILs.

Now, the only left out part in the proceeding discussion was on conductivity, the term quantifies the charge transport mechanisms. Considering its importance to technological applications and the fundamental significance to glassy dynamics, researchers had been in the pursuit of modelling it with different empirical relations. As early as in 1970s Barton–Nakajima–Namikawa proposed a model (BNN model) connecting dc conductivity σ_0 and ω_e based on Einstein and Einstein–Smoluchowski equations, arriving an approximate relation for the dc conductivity as [2,40,41]

$$\sigma_0 = nqu = n\frac{q^2D}{KT} = n\frac{q^2}{KT}\frac{\lambda^2}{2\tau_h} = n\frac{q^2}{KT}\frac{\lambda^2\omega_e}{2}$$

where n is the effective number density of ions, q is the elementary charge and D is the diffusion coefficient ($D = \frac{\lambda^2\omega_e}{2}$, where λ is the hopping length of charge carriers and τ_h is the hopping time, $\tau_h \sim \tau_e = {}^1/_{\omega e}$). Here, σ_0 and ω_e are the observable quantities characterizing charge transport in ILs. A very good correlation was observed in the case of the ILs as depicted in Fig. 10. Further, on comparing the conductivity at ambient conditions, these phosphonium ILs can solve most of the

Table III
Fit parameters obtained from VFT equation of three phosphonium based ILs.

Samples	log τ_0 (s)	B (K)	T_0 (K)	T_g (BDS) (K)	T_g (DSC) (K)	Fragility (m)	Activation Energy (E_β) (kJ/mol)
$[PC_6C_6C_6C_{14}]$ $[NTf_2]$	9.65	585.23	165.33	185.75	193.02	113.30	46.53
$[PC_6C_6C_6C_{14}]$ $[N(CN)_2]$	9.83	708.84	166.31	190.68	195.99	98.78	34.65
$[PC_6C_6C_6C_{14}]$ [Cl]	9.39	718.80	169.43	195.03	202.82	92.86	33.68

shortcomings raised against the conventional electrolytes (aqueous and organic) for electrochemical applications. We had already reported the results of electrochemical investigations by fabricating supercapacitors by choosing appropriate active electrodes and these ILs as electrolytes [2,42–44]. It is worth to mention that by using the IL electrolytes, we could enhance the operating voltage window to about 4 V from the conventional upper limit of 1 V by keeping all the virtues and good features of ILs (non-flammability, have low melting point, low volatility, and high thermal stability) [2,42–44].

3.5. In silico analysis and biological evaluations

The pharmaceutical industry is facing many challenges in the discovery of novel and effective drugs and their consequent therapeutic applications [15]. Approximately 50% of available drugs are administered as crystalline form having low bioavailability resulting from poor solubility, low thermal and chemical stability, adverse effects from polymorphism *etc*. Converting the crystalline drug into IL is a promising pathway for bypassing many of above mentioned shortcomings [15]. Several studies have reported the usefulness of ILs in biomedical applications as anti-bacterial, anti-oxidant and anti-cancer agents [15–22]. Arising curiosity from these investigations, we have pursued the above with the three ILs. We began our investigations with *in silico* analysis on the three ILs to extract pharmacokinetic profiles with well validated ADMET (absorption, distribution, metabolism, excretion and toxicity) prediction tools [25,26]. The other analytical examinations can be followed after getting proper hints about the ILs. The results of *in silico* analysis are given in Tables IV and V, showing the drug likeness indices and toxicity parameters within the permissible limits.

3.5.1. Anti-bacterial activity

The *in vitro* anti-bacterial activity of the three ILs were investigated against two bacterial strains *E. coli* (gram negative) and *S. aureus* (gram positive) at different concentrations by agar disc diffusion method as detailed in the experimental section [14,16]. The results were analyzed by measuring the width of zone of inhibition against the bacterial strains and given in Table VI. Ferraz et al., evaluated the anti-bacterial activities of novel active pharmaceutical ingredient ionic liquids (API–ILs) based on ampicillin anion [Amp] and showed growth

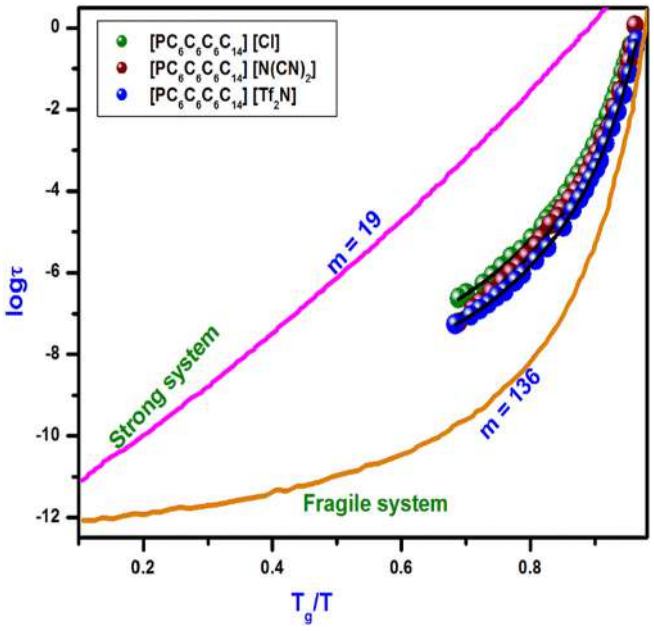

Fig. 9. Angell plot depicting log τ(s) *vs* T_g/T [39].

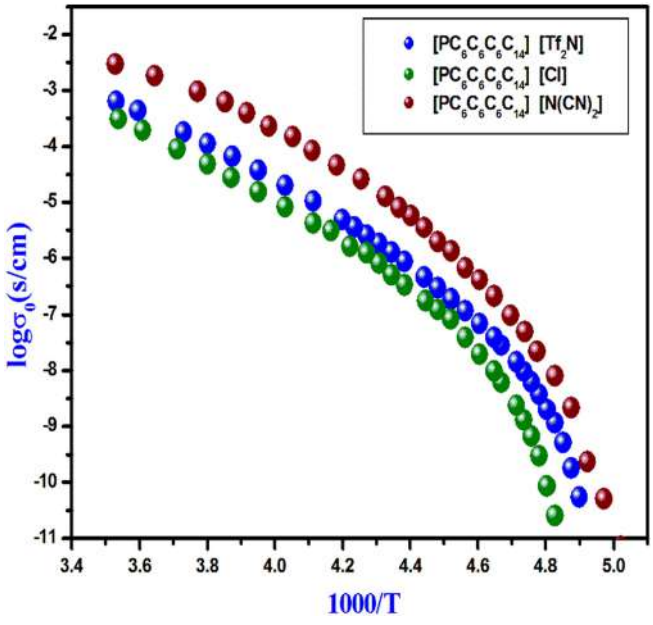

Fig. 8. Plots of 1000/T (K^{-1}) *vs* log σ (S/cm) of the three ILs.

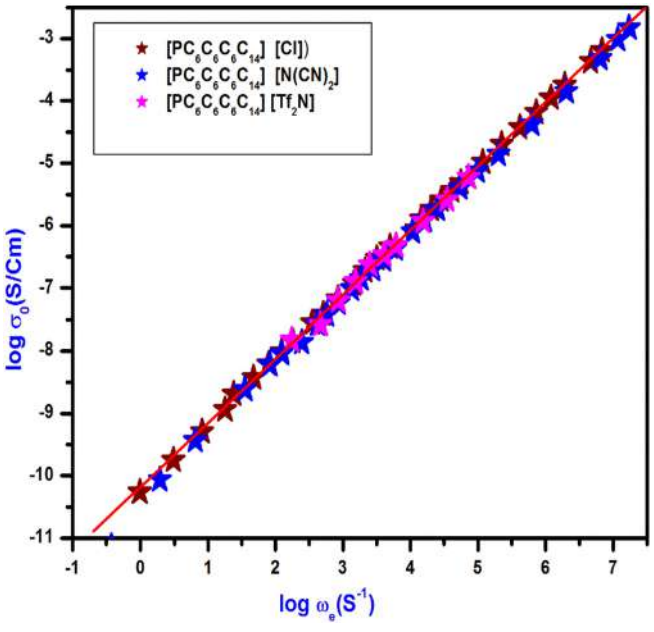

Fig. 10. BNN plot (log σ_0 *versus* log ω_e) of the three ILs.

Table IV
In silico predictions on physico-chemical and drug likeness properties of three phosphonium based ILs.

Ionic liquid	MW (g/mol)	Physicochemical properties				Drug likeness					
		TPSA	O/NH	VIOL	VOL	GPC	ICM	KI	NRL	PI	EN
$[PC_6C_6C_6C_{14}]$ $[NTf_2]$	764	71.52	0	2	715	−0.25	−0.95	−0.77	−0.69	0.05	−0.52
$[PC_6C_6C_6C_{14}]$ $[N(CN)_2]$	550	50.82	0	2	623	0.14	0.07	0.01	−0.04	0.30	0.23
$[PC_6C_6C_6C_{14}]$ [Cl]	519	0.00	0	2	590	0.14	0.15	0.00	0.01	0.20	0.17

TPSA: total polar surface area, O/NH: O-HN interaction, VIOL: number of violation, VOL: volume, GPC: GPCR ligand, ICM: ion channel modulator, KI: kinase inhibitor, NRL: nuclear receptor ligand, PI: protease inhibitor, EI: enzyme inhibitor.

Table V
In silico screening of predicted LD_{50} and toxicity profiles of three phosphonium based ILs.

Ionic liquid	AMES toxicity	Rat acute toxicity LD_{50} (mol/kg)	Bioavailability score
$[PC_6C_6C_6C_{14}]$ $[NTf_2]$		2.81	0.17
$[PC_6C_6C_6C_{14}]$ $[N(CN)_2]$		2.26	0.55
$[PC_6C_6C_6C_{14}]$ [Cl]		2.33	0.17

: Non-toxic; : Toxic.

inhibition and bactericidal properties on some gram-negative resistant bacteria [14]. Doria et al. studied the bacterial growth inhibition halos at different imidazolium based ILs with different concentrations in agar well diffusion assay [45]. The accumulated data on the biological activity of ILs, including their anti-microbial and cytotoxic properties, are discussed in view of possible applications in drug synthesis and drug delivery systems. As given in the Table VI, the anti-bacterial activity of the three ILs against *E. coli* is slightly higher than that against *S. aureus*. Further, it is found that phosphonium based IL with $[N(CN)_2]^-$ anion showed the highest activity followed by $[NTf_2]^-$ and the least with $[Cl]^-$ displaying that antibacterial activity shows a correlation with the ionic conductivity.

3.5.2. Anti-oxidant activity

The IC_{50} concentration which is required to obtain a 50% DPPH scavenging anti-oxidant effect was determined and is used to compare the anti-oxidant capacity of the three ILs. The results on the three ILs along with ascorbic acid (as standard) are shown in Table VII. The lower IC_{50} value indicates higher anti-oxidant activity and accordingly, IL with $[NTf_2]^-$ anion showed the highest anti-oxidant activity followed by $[Cl]^-$ and the least with $[N(CN)_2]^-$.

Table VI
Anti-bacterial activity of three phosphonium based ILs with different concentration against *S. aureus* and *E. coli.*

Ionic liquids	Concentration of IL (μg/ml)	Diameter of zone of inhibition (mm)	
$[PC_6C_6C_6C_{14}]$ $[NTf_2]$	0	0.3	0.2
	2.5	13.5	10.6
	5	17.3	14.3
	7.5	20.4	17.2
	10	21.4	19.5
	12.5	23.4	21
$[PC_6C_6C_6C_{14}]$ $[N(CN)_2]$	0	0.5	0.5
	2	14.5	12.6
	4	17.4	15.3
	6	21	19.4
	8	23	21.3
	10	25.4	22.7
$[PC_6C_6C_6C_{14}]$ [Cl]	0	0.4	0.3
	2.5	12.6	9.8
	5	18.5	14.4
	7.5	22.1	19.4
	10	25.2	21.2

3.5.3. In vitro cytotoxicity assay

The cytotoxicity studies on the ILs against four cell lines (A549, K562, Jurkat E6-1 and HCT 116) were carried out using a standard assay, 3-(4,5-dimethylthiazol-2-yl)-2,5-diphenyltetrazolium bromide (MTT). The percentage cell viability is determined to evaluate the activity over the cell lines vis-à-vis on untreated cells as control. The concentration of IL which can cause 50% of cell death (IC_{50}) can ascertain the quantitative analysis on its cytotoxic effect. The results were shown in Table VIII. Lower the IC_{50} values, more cytotoxic is the IL used. $[PC_6C_6C_6C_{14}][Cl]$ showed lower IC_{50} values in K562, Jurkat E6-1, HCT 116 cell lines, while $[PC_6C_6C_6C_{14}][N(CN)_2]$ is more effective in A549 cell line. The results show that the anion play a significant role on its affinity towards various cell lines resulting in specific cytotoxicity against different cancer cells. Malhotra et al. studied the anti-cancer activity and cytotoxicity of imidazolium, phosphonium and ammonium-based ionic liquids (ILs) in 60 human tumor cell lines and found that phosphonium-based ILs were found to be more active and less cytotoxic as compared to ammonium ILs [21,22].

4. Conclusions

Three phosphonium based ILs were investigated with trihexyltetradecylphosphonium ($[PC_6C_6C_6C_{14}]$) as cation and chloride $[-Cl]^-$, dicyanamide $[-N(CN)_2]^-$ and bis(trifluoromethyl sulfonyl)

Table VII
The anti-oxidant activity of the three ILs.

Samples	IC_{50} values (mM)
$[PC_6C_6C_6C_{14}][NTf_2]$	0.28 ± 6.93
$[PC_6C_6C_6C_{14}][Cl]$	9.11 ± 0.15
$[PC_6C_6C_6C_{14}][N(CN)_2]$	551.7 ± 14.5
Ascorbic acid	0.0227 ± 0.31

Table VIII
The IC_{50} values calculated for four cell lines with the ILs.

Cell lines	IC_{50} values		
	$[PC_6C_6C_6C_{14}][NTf_2]$ (μM)	$[PC_6C_6C_6C_{14}]$ [Cl] (μM)	$[PC_6C_6C_6C_{14}][N(CN)_2]$ (μM)
K562	241.9 ± 2.4	40 ± 5.3	175 ± 6.2
Jurkat E6-1	160.8 ± 5.2	23.75 ± 2.4	146.25 ± 7.2
HCT 116	503.11 ± 2.6	107.5 ± 5.1	288 ± 4.8
A549	40 ± 2.1	36 ± 3.4	25 ± 2.2

imide [-NTf_2]$^-$ as anions to extract the effect of size, symmetry, dipole moment and electro-negativity of anions on charge transport, glassy dynamics *via* experimental and computational means. The DSC, TGA measurements pointed that the ILs to be good heat transfer fluid for electrolytic and high temperature applications with improved thermal stability up to 573 K. The dielectric measurements revealed that the conductivity relaxation follows Dyre's random barrier model arising due to the hopping of charge carriers in a random spatially varying potential landscape following a Vogel–Fulcher–Tamman (VFT) T-dependance. The sub-Tg relaxation followed a Cole-Cole response with an Arrhenius T-dependence. A cation influenced dynamics was further revealed with Tg correlates with size, while anticorrelating with the fragility and low temperature activation energy (E_β). The structure and other parameters revealed from the experimental invstigationsof FT-IR and FT-Raman are well matched with the values obtained from DFT studies. Pharmacokinetics, bioavailability and toxicity studies *via in silico* analysis revealed that the ILs fulfilled most of the requirements needed for the pharmaceutical applications. On exploring the biological applications, the ILs showed very good anti-bacterial, anti-oxidant and anti-cancer activity highlighting their significance for pharmaceutical industry.

CRediT authorship contribution statement

K.K. Thasneema: Investigation, Formal analysis, Writing – original draft. **M. Shahin Thayyil:** Supervision, Writing - review & editing. **Tancia Rosalin:** Investigation. **K.K. Elyas:** Investigation. **T. Dipin:** Formal analysis. **Pramod K. Sahu:** Formal analysis. **N.S. Krishna Kumar:** Formal analysis. **V.C. Saheer:** Formal analysis. **Mouslim Messali:** Formal analysis. **Taibi Ben Hadda:** Formal analysis.

Declaration of competing interest

The authors declare that there is no conflict of interest.

Acknowledgements

The authors gratefully acknowledge A. Afsal for his supports in the dielectric measurements and Jayant Kolte for fruitful discussions. T.K.K. acknowledges the UGC, Govt. of India for financial assistance through BSR fellowship. MST acknowledges research funding from the KSCSTE, Govt. of Kerala, India (No. 005/SRSPS/2011/CSTE and No. 49/SARD/2014), and the UGC, Govt. of India (MRP F. No. 42-848/2013 (SR)). The CSIF, University of Calicut is acknowledged for providing sophisticated experimental facilities. Tancia Rosalin acknowledges UGC for MANF fellowship, Department of Biotechnology, Govt. of India and University of Calicut for the infrastructural facilities.

Appendix A. Supplementary data

Supplementary data to this article can be found online at https://doi.org/10.1016/j.molliq.2020.112960.

References

[1] Jan Leys, Michael Wübbenhorst, Chirukandath Preethy Menon, Ravindran Rajesh, Jan Thoen, Christ Glorieux, Temperature dependence of the electrical conductivity of imidazolium ionic liquids, J. Chem. Phys. 128 (2008), 064509.
[2] K.K. Thasneema, P. Shabeeba, Mohamed Shahin Thayyil, Mahadevan Pillai, N.S. Krishna Kumar, G. Govindaraj, V.C. Saheer, M.P. Nighil Nath, Dielectric relaxation and electrochemical studies on trihexyl tetradecyl phosphonium chloride ionic liquid, J. Mol. Liq. 252 (2018) 488–494.
[3] Subbiah Sowmiah, Venkatesan Srinivasadesikan, Ming-Chung Tseng, Yen-Ho Chu, On the chemical stabilities of ionic liquids, Molecules 14 (2009) 3780–3813.
[4] Kyoko Fujita, Douglas R. MacFarlane, Maria Forsyth, Protein solubilising and stabilising ionic liquids, Chem. Commun. (2005) 4804–4806.
[5] Bronya Clare, Amal Sirwardana, Douglas R. MacFarlane, Synthesis, purification and characterization of ionic liquids, Top. Curr. Chem. 290 (2009)Springer-Verlag Berlin Heidelberg.
[6] Hiroyuki Tokuda, Kikuko Hayamizu, Kunikazu Ishii, Md. Abu Bin Hasan Susan, Masayoshi Watanabe, Physicochemical properties and structures of room temperature ionic liquids. 1. Variation of anionic species, J. Phys. Chem. B 108 (2004) 16593–16600.
[7] Wu Xu, Emanuel I. Cooper, C. Austen Angell, Ionic liquids: ion mobilities, glass temperatures, and fragilities, J. Phys. Chem. B 107 (2003) 6170–6178.
[8] Kazuhide Ueno, Zuofeng Zhao, Masayoshi Watanabe, C. Austen Angell, Protic ionic liquids based on decahydroisoquinoline: lost super fragility and ionicity-fragility correlation, J. Phys. Chem. B 116 (2012) 63–70.
[9] Joshua R. Sangoro, Friedrich Kremer, Charge transport and glassy dynamics in ionic liquids, Acc. Chem. Res. 45 (4) (2012) 525–532.
[10] A. Rivera, A. Brodin, A. Pugachev, E.A. Rossler, Orientational and translational dynamics in room temperature ionic liquids, J. Chem. Phys. 126 (2007), 114503.
[11] J. Leys, et al., Influence of the anion on the electrical conductivity and glass formation of 1-butyl-3-methylimidazolium ionic liquids, J. Chem. Phys. 133 (2010), 034503.
[12] Elzbieta Frackowiak, Gregorz Lota, Juliusz Pernak, Roomtemperature phosphonium ionic liquids for super capacitor applications, Appl. Phys. Lett. 86 (2005), 164104.
[13] Kris Anderson, Hector Rodriguez, Kenneth R. Seddon, Phase behavior of trihexyl (tetradecyl) phosphonium chloride, nonane and water, Green Chem. 11 (2009) 780–784.
[14] Ricardo Ferraz, Vˆania Teixeira, D 'ebora Rodrigues, R 'uben Fernandes, Cristina Prudˆencio, Joˆao Paulo Noronha, Zeljko Petrovski, Luıs C. Branco, Antibacterial activity of ionic liquids based on ampicillin against resistant bacteria, RSC Adv. 4 (2014) 4301–4307.
[15] Ana Rita Dias, Joao Costa-Rodrigues, Maria Helena Fernandes, Ricardo Ferraz, Cristina Prudencio, The anticancer potential of ionic liquids, ChemMedChem 12 (2017) 11–18.
[16] P. Mozhiyarasi, R. Anuradha, A study on phytochemical analysis and antimicrobial activity of Hyptis suaveolens (L.) poit, J. Chem. Pharm. Res. 8 (6) (2016) 438–442.
[17] S. Chanda, R. Dave, M. Kaneria, In vitro antioxidant property of some Indian medicinal plants, J. Med. Plant Res. 5 (2) (2011) 169–179.
[18] Prakash Veeru, Mishra Pankaj Kishor, Mishra Meenakshi, Screening of medicinal plant extracts for antioxidant activity, J. Med. Plant Res. 3 (8) (2009) 608–612.
[19] W. Brand-Williams, M.E. Cuvelier, C. Berset, Use of free radical method to evaluate antioxidant activity, Lebensm Wiss U Technol 28 (1995) 25–30.
[20] Nur Afiqah Ahmad, Khairulazhar Jumbri, Anita Ramli, Noraini Abd Ghani, Haslina Ahmad, Mohd Azlan Kassimd, Synthesis, characterisation and antioxidant properties of ferulate-based protic ionic liquids: experimental and modelling approaches, J. Mol. Liq. 278 (2019) 309–319.
[21] Sanjay V. Malhotra, Vineet Kumar, A profile of the in vitro anti-tumor activity of imidazolium based ionic liquids, Bioorg. Med. Chem. Lett. 20 (2010) 581–585.
[22] Vineet Kumar, Sanjay V. Malhotra, Study on the potential anti-cancer activity of phosphonium and ammonium-based ionic liquids, Bioorg. Med. Chem. Lett. 19 (2009) 4643–4646.
[23] N. Murugan,a L. Kavitha,c E. Shinyjoy,a D. Rajeswari,d K. Vimala,e S. Kannane and D. Gopi, Smart rose flower like bioceramic/metal oxide dual layer coating with enhanced anti-bacterial, anticancer, anti-corrosive and biocompatible properties for improved orthopedic applications, RSC Adv., 5, 85831–85844 (2015).
[24] Thondhi Ponraj, Manickam Paulpandi, Raju Vivek, Karuppaiya Vimala, Soundarapandian Kannan, Protein regulation and apoptotic induction in human breastcarcinoma cells (MCF-7) through lectin from G. beauts, Int. J. Biol. Macromol. 95 (2017) 1235–1245.
[25] Nadjet Rezki, Salsabeel A. Al-Sodies, Mouslim Messali, Sanaa K. Bardaweel, Pramod K. Sahu, Fawzia F. Al-blewi, Praveen K. Sahu, Mohamed R. Aouad, Identification of new pyridinium ionic liquids tagged with Schiff bases:design, synthesis, in silico ADMET predictions and biological evaluations, J. Mol. Liq. 264 (2018) 367–374.
[26] Mouslim Messali, Mohamed R. Aouad, Wael S. El-Sayed, Adeeb Al-Sheikh Ali, Taibi Ben Hadda, Belkheir Hammouti, New eco-friendly 1-alkyl-3-(4-phenoxybutyl) imidazolium-based ionic liquids derivatives: a green ultrasound-assisted synthesis, characterization, antibacterial activity and POM analyses, Molecules 19 (2014) 11741–11759.
[27] Maria Villanueva, Alberto Coronas, Josefa Garcia, Josefa Salgado, Thermal stability of ionic liquids for their application as new absorbents, Ind.Eng.Chem.Res 52 (2013) 15718–15727.
[28] Léa Chanceliera, Olivier Boyrona, Thibaut Gutelb, Catherine C. Santinia, Thermal stability of imidazolium-based ionic liquids, French-Ukrainian J. Chem. Volume 04 (Issue 01) (2016).
[29] Fathy A. Yassin, Fathy Y. El Kady, Hoda S. Ahmed, Latifa K. Mohamed, Seham A. Shaban, Ahmed K. Elfadaly, Highly effective ionic liquids for biodiesel production from waste vegetable oils, Egypt. J. Pet. 24 (2015) 103–111.
[30] C. Krause, J.R. Sangoro, C. Iacob, F. Kremer, Charge transport and dipolar relaxations in imidazolium-based ionic liquids, J. Phys. Chem. B 114 (2010) 382–386.
[31] Z. Wojnarowska, et al., Molecular dynamics studies on the water mixtures of pharmaceutically important ionic liquid lidocaine HCl, Mol. Pharm. 9 (2012) 1250–1261.
[32] K.P Safna Hussan, M. Shahin Thayyil, S.K. Deshpande, T.V Jinitha, K. Manoj, K.L. Ngai, Molecular dynamics and the translational–rotational coupling of an ionically conducting glass-former: amlodipine besylate, RSC Adv. 8 (2018) 20630–20636.
[33] F. Kremer, A. Schonhals, Broadband Dielectric Spectroscopy, ISBN 3-540-43407-0 Springer-Verlag, Berlin Heidelberg New York, 2003.
[34] K.P Safna Hussan, M. Shahin Thayyil, V.K. Rajan, Anu Antony, The interplay between charge transport and CO2 capturing mechanism in [EMIM][SCN] ionic liquid: a broadband dielectric study, J. Phys. Chem. B 123 (2019) 6618–6626.
[35] J. Sangoro, et al., Electrical conductivity and translational diffusion in the 1-butyl-3-methylimidazolium tetrafluoroborate ionic liquid, J.chem.phys 128 (2008), 214509.

[36] U. Sailaja, M. Shahin Thayyil, N.S.K. Kumar, G. Govindaraj, European Journ al of Pharm aceutical Sciences Molecular dynamics in liquid and glassy states of non-steroidal anti-inflammatory drug: ketoprofen, Eur. J. Pharm. Sci. 49 (2013) 333–340.
[37] C.A. Angell, K.L. Ngai, G.B. McKenna, P.F. McMillan, S.W. Martin, Relaxation in glassforming liquids and amorphous solids, J. Applied Phys. 88 (2000) 3113–3157.
[38] H. Tanaka, Two-Order-Parameter Description of Liquids. I. A General Model of Glass Transition Covering its Strong to Fragile Limit Two-Order-Parameter Description of Liquids. I A General Model of Glass Transition Covering its Strong to Fragile Limit, 2012 3163.
[39] R. Bohmer, K.L. Ngai, C.A. Angell, D.J. Plazek, Nonexponential relaxations in strong and fragile glass formers, J. Chem. Phys. 99 (1993) 4201.
[40] J.R. Sangoro, C. Iacob, A. Serghei, C. Friedrich, F. Kremer, Universal scaling of charge transport in glass-forming ionic liquids, Phys. Chem. Chem. Phys. 11 (2009) 913–916.
[41] C. Iacob, J.R. Sangoro, W.K. Kipnusu, R. Valiullin, J. Karger, F. Kremer, Enhanced charge transport in nano-confined ionic liquids, Soft Matter 8 (2012) 289–293.
[42] S. Pilathottathil, K.K. Thasneema, M. Shahin Thayyil, M.P. Pillai, C.V. Niveditha, A high voltage supercapacitor based on ionic liquid with an activated carbon electrode, Mater. Res. Express 4 (2017).
[43] P. Shabeeba, K.K. Thasneema, M. Shahin Thayyil, M.P. Pillai, C.V. Niveditha, A graphene-based flexible supercapacitor using trihexyl (tetradecyl) phosphonium bis (trifluoromethanesulfonyl) imide ionic liquid electrolyte, Mater. Res. Express 4 (2017).
[44] S. Pilathottathil, T. Kannan, M. Shahin Thayyil, Inorganic salt grafted ionic liquid gel electrolytes for ef fi cient solid state supercapacitors: electrochemical and dielectric studies, J. Mol. Liq. 264 (2018) 72–79.
[45] Oscar Forero Doria, Ricardo Castro, Margarita Gutierrez, Diego Gonzalez Valenzuela, Leonardo Santos, David Ramirez, Luis Guzman, Novel alkylimidazolium ionic liquids as an antibacterial alternative to pathogens of the skin and soft tissue infections, Molecules 23 (2018) 2354.